

# Learning Intra- and Inter-Cell Differences for Accurate Battery Lifespan Prediction across Diverse Conditions

Han Zhang<sup>1\*</sup>, Yuqi Li<sup>2\*</sup>, Shun Zheng<sup>3</sup>, Ziheng Lu<sup>3</sup>, Xiaofan Gui<sup>3</sup>, Wei Xu<sup>1</sup>, Jiang Bian<sup>3</sup>

<sup>1</sup>Institute for Interdisciplinary Information Sciences, Tsinghua University

<sup>2</sup>Department of Materials Science and Engineering, Stanford University

<sup>3</sup>Microsoft Research

## Abstract

Battery life prediction holds significant practical value for battery research and development. Currently, many data-driven models rely on early electrical signals from specific target batteries to predict their lifespan. A common shortfall is that most existing methods are developed based on specific aging conditions, which not only limits their model’s capability but also diminishes their effectiveness in predicting degradation under varied conditions. As a result, these models often miss out on fully benefiting from the rich historical data available under other conditions. Here, to address above, we introduce an approach that explicitly captures differences between electrical signals of a target battery and a reference battery, irrespective of their materials and aging conditions, to forecast the target battery life. Through this inter-cell difference, we not only enhance the feature space but also pave the way for a universal battery life prediction framework. Remarkably, our model that combines the inter- and intra-cell differences shines across diverse conditions, standing out in its efficiency and accuracy using all accessible datasets. An essential application of our approach is its capability to leverage data from older batteries effectively, enabling newer batteries to capitalize on insights gained from past batteries. This work not only enriches the battery data utilization strategy but also sets the stage for smarter battery management system in the future.

## 1 Main

Lithium-ion batteries are central to the energy transition, propelling the surge of renewable energy solutions and electric vehicles, owing to their high energy density and cyclic reliability. Predicting their lifespan accurately is paramount for applications where cost and reliability are crucial. Data-driven strategies combining machine learning and expert insights have recently advanced early-stage battery lifetime predictions. Based on the *intra-cell* difference between the voltage-capacity curves of the cycles in the early degradation stage, linear models for the first time reveals the relationship between the electrical signals and the lifespan of lithium-iron phosphate cells. In this vein, considerable efforts have

been made to enhance prediction performance by developing more representative features and utilizing stronger models.

However, due to the high data acquisition cost, existing studies merely cover a relatively small number of battery instances and often focus on specific material composition or operating conditions. This singular focus overlooks the opportunities of utilizing the vast historical data from heterogeneous battery types, not only impeding their prediction potential in the target aging situation, but also reducing their generalization performance across varied conditions. Thus, when dealing with complex aging conditions at a larger scale, the models tailored for specific scenarios will struggle to generalize due to the diverse degradation patterns and become inclined to overfit on data noise and outliers. These limitations underscore the need for a more holistic, robust, and universally applicable prediction framework.

To bridge this gap, we introduced the *inter-cell* difference for any target-reference battery pair to explicitly characterizes the electrical signal variations, and then proposed a framework that utilizes both the intra- and inter-cell difference features simultaneously. Compared with the existing methods based solely on the intra-cell difference, the additional inter-cell difference significantly enrich the feature space, offering a more adaptable and data-efficient battery life prediction model through flexible target-reference battery comparisons. Further decoupling mechanism analysis highlights the unique advantages of inter-cell features in predictive capabilities. Notably, this novel methodology harnesses the insights gleaned from historical battery data, allowing newer battery designs to benefit from past experiences. This pioneering approach promises to redefine the landscape of battery life prediction.

## 2 The BatDiff lifetime prediction framework

Previous battery lifetime prediction methods rely on the *intra-cell difference* (IntraCD) features of voltage-capacity curves, utilizing a specific cycle of the target battery as the reference signal (upper Figure 1a). However, such IntraCD-based methods fail to harness the information across diverse battery instances. As a result, they usually experience a sub-optimal data utilization and are susceptible to overfitting in data-scarce scenarios. Here we propose the utilization of *inter-cell difference* (InterCD) features to directly leverage

\* Equal contribution. This work was done during the internship at Microsoft Research.

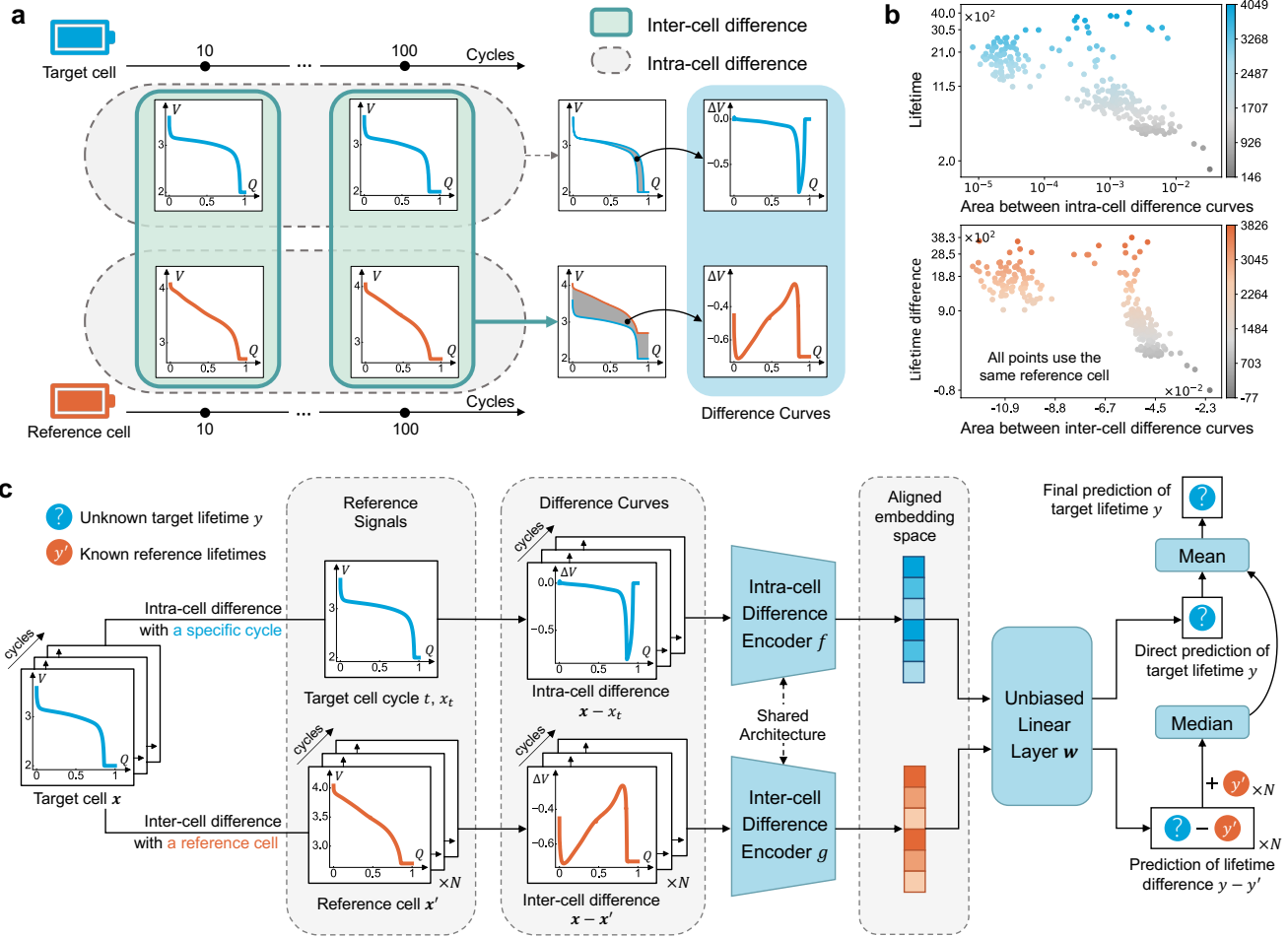


**Figure 1.** Inter-cell difference features and the BatDiff framework. The target cells (blue) are lithium iron phosphate (LFP) battery, and the reference cell (orange) is a lithium cobalt oxide (LCO) battery. **a:** Illustration of intra- and inter-cell difference features. **b:** Both intra- and inter-cell difference features demonstrate a high correlation with the battery lifetime. Each point in the both figures represents a battery cell. **c:** The architecture of the BatDiff framework.

the interrelation between batteries for lifetime prediction. InterCD features use a battery cell of any type as reference and take the signal differences between the corresponding cycles of the two cells. Different from IntraCD features, InterCD curves encode the rich degradation information of both batteries and are much more diverse due to the flexible combinations. Figure 1a gives an illustration of the IntraCD and InterCD features.

Both IntraCD and InterCD features in early stages have direct correlation with the battery lifetime. The upper of Figure 1b shows that the area between the intra-cell voltage-capacity curves is highly correlated with its lifespan, where a larger area indicates a faster battery degradation and thus a shorter lifespan [9]. The lower of Figure 1b shows that the area between the voltage-capacity curves of two batteries also reflects their lifetime difference, with a larger area indicating a larger lifespan difference. This verifies that a

statistical model can be learned to predict the lifetime difference between two batteries given the InterCD features. Furthermore, the target lifetime is naturally implied when the lifetime of the reference cell is known. Note that while the IntraCD displays a linear relationship with the battery lifetime, the correlation between the InterCD features and the lifetime difference is clearly non-linear and thus it requires stronger models for pattern recognition.

InterCD significantly improves the data utilization and allows additional performance improvement through reference ensembles. Approaches based on IntraCD often necessitate careful early stopping to prevent potential overfitting in data-scarce scenarios. In contrast,  $N(N-1)$  ordered input pairs can be constructed for InterCD features from  $N$  batteries, which significantly alleviates the data-scarcity issue. During inference, combining the predictions from different reference cells offers an opportunity to further improve

the predictive performance. This performance enhancement achieved through the reference ensembles is a unique advantage of InterCD, and is orthogonal to other techniques such as data augmentation and model ensembles.

The IntraCD- and InterCD-based approaches can be naturally combined under a contrastive learning framework for accurate and robust lifetime prediction across different battery types and operating conditions. Since the two approaches predict the same target lifespan based on different feature spaces, it is beneficial to align their embedding spaces to allow mutual regularization and enhancement. In fact, we can prove that their embedding spaces are perfectly aligned under certain specifications<sup>1</sup>. In practice, we employ two separate encoders of the same architecture to capture the distinct aging patterns in IntraCD and InterCD features into an aligned embedding space. Then, a shared linear regression layer produces the predictions of the battery lifetime for IntraCD branch or the estimations of lifetime differences for the InterCD branch. The result framework, named as the *BatDiff* framework, explicitly connects the optimization of IntraCD and InterCD-based predictors and enjoy their mutual complementarity for better predictive performance. Figure 1c depicts the complete pipeline.

To encompass the complete degradation information of the battery, we calculate six capacity-indexed feature curves as raw input signals. We compute the current-capacity and voltage-capacity curves during both charge and discharge periods by linearly interpolating the raw time series signals. We further derive the differential voltage curve and the resistance curve with the composition of the four computed curves. The capacity range of these curves is normalized to [0, 1] with respect to its nominal capacity for proper calculation of inter-cell differences. Please refer to the Method section for further details.

### 3 BatDiff Ensures Accurate Predictions across Aging Conditions

We curated, to the best of our knowledge, all the existing battery data suitable for early battery life prediction to comprehensively evaluate our method in comparison with existing approaches. Six distinct test datasets covering various of battery models and operating conditions are constructed for experimentation.

MATR-1 and MATR-2 [9] consist of 123 commercial 18650 lithium-ion phosphate/graphite (LFP) batteries. All batteries share the same discharging protocol but are charged at different rates. MATR-2 requires the model to generalize to different charging protocols while the training and test dataset of MATR-1 follow the same distribution. We construct MATR-full that includes all the batteries from MATR-1 and MATR-2, as well as additional 55 LFP 18650 cells cycled with the optimized charging protocols [1] to assess how the model

generalizes across diverse data batches obtained at different time points. The HUST dataset [7] involves 77 LFP batteries with a constant charging protocol but different discharge speeds. All the cells in these four datasets belong to the same battery model.

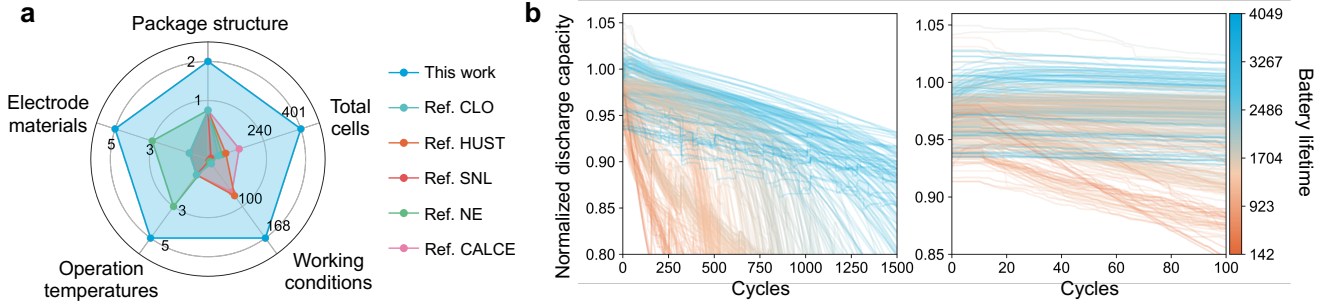
Additionally, we collected batteries used in prior studies including CALCE [4, 10, 11], HNEI [3], UL-PUR [5], RWTH [6] and SNL [8]. By combining these batteries with MATR-full and HUST, we obtained a total collection of 401 batteries. To evaluate the performance under different lifetime prediction scenarios, we developed two test datasets MIX-20 and MIX-100. In MIX-20, the models are required to predict the cycles before degradation to 90% of the nominal capacity, using the data from only the first 20 cycles. In MIX-100, the models predict the 80% end of life point using data from the first 100 cycles. Notably, batteries that had already degraded to the end of life during the early cycles were excluded in the experiments.

Figure 2a shows that the collected dataset exhibits a more comprehensive coverage that goes beyond the confines of previous works. Figure 2b further visualizes the capacity degradation of the collected batteries in the first 1500 and 100 cycles of the batteries. Here the long-term degradation is highly non-linear and demonstrates considerable variation among batteries. In contrast, the degradation within the initial 100 cycles remains indiscernible for most batteries. Such diverse and intricate characteristics require the model to capture and distinguish the degradation patterns caused by various factors for generalization.

Table 1 presents the comparison results of the proposed methods against various baselines on these six datasets. Employing only the InterCD method achieves superior performance on MATR-1, MATR-full and HUST. This indicates that the model effectively captures the degradation patterns of the LFP cells under different charging and discharging protocols. InterCD shows even larger performance advantage in comparison with the baselines on MIX-20 and MIX-100. This phenomenon arises due to the tendency of the IntraCD-based baselines to underfit or even diverge as they encounter an increasing variety of battery types. In contrast, the InterCD adeptly captures the diverse degradation patterns, thus yielding more accurate predictions. The InterCD method demonstrates a suboptimal performance of the InterCD method on MATR-2. Figure S2 indicates the cause is that several battery cells with long lifespans resemble the electrical signals of batteries with much smaller lifetimes. Figure S3 shows both IntraCD and InterCD underestimate the lifespans of these batteries, and InterCD makes bolder predictions due to their high similarity with short-lifespan batteries, as visualized by Figure S4.

With the joint training of IntraCD and InterCD branches, BatDiff further boosts the prediction performance over InterCD alone, leading to the lowest prediction errors on all

<sup>1</sup>Please refer to the Method section for details.



**Figure 2.** Visualization of datasets. **a:** The coverage of the dataset employed in this work significantly surpasses that of previous undertakings. **b:** A visualization of the capacity degradation with respect to the cycles for all the cells. The curves are normalized by their nominal capacities. The first 1500 and 100 cycles are shown. The degradation patterns are highly non-linear and are difficult to distinguish in the first 100 cycles.

Method	MATR-1		MATR-2		MATR-full		HUST		MIX-20		MIX-100	
	RMSE	MAPE(%)	RMSE	MAPE(%)	RMSE	MAPE(%)	RMSE	MAPE(%)	RMSE	MAPE(%)	RMSE	MAPE(%)
Training Mean	399	28	511	36	331	31	420	18	593	102	573	59
“Variance” Model[9]	138	15	196	12	179	17	398	17	601	95	521	39
“Discharge” Model[9]	86	8	173	11	144	14	322	14	>2000	>100	1743	47
“Full” Model[9]	100	11	214	12	139	14	335	14	441	53	331	22
Ridge Regression[2]	125	13	188	11	178	13	1047	36	806	150	395	30
PCR[2]	100	11	176	11	173	13	435	19	701	78	384	28
PLSR[2]	97	10	193	11	168	13	431	18	543	77	371	26
SVM Regression	140	15	300	18	145	11	344	16	438	46	257	18
Random Forest[2]	140	15	202	11	203	16	348	16	288	31	211	14
MLP[2]	162±7	12±0	207±4	11±0	165±5	12±1	444±5	18±1	532±25	61±6	455±37	27±1
LSTM	123±11	12±2	226±36	14±2	200±21	14±1	442±32	20±1	417±62	37±7	266±11	15±1
CNN[2]	115±96	9±6	237±107	17±8	223±72	15±3	445±35	21±1	785±132	41±4	261±38	15±1
InterCD	73±3	7±0	260±13	17±1	109±7	10±1	265±10	10±1	210±15	18±1	181±13	12±1
BatDiff	<b>59±2</b>	<b>6±0</b>	<b>163±12</b>	<b>11±1</b>	<b>85±8</b>	<b>7±1</b>	<b>264±9</b>	<b>10±1</b>	<b>201±18</b>	<b>18±1</b>	<b>158±7</b>	<b>10±0</b>

**Table 1.** Comparison results with baseline methods. We employ bold font to emphasize the best-performing method and utilize underlines to denote the second-best baselines. For neural-network-based methods, we report the mean and standard deviation of eight random seeds.

datasets. It is important to note that, no method prior to BatDiff has managed to consistently achieve optimal performance across all datasets. BatDiff reduced the root mean square error (RMSE) over the second-best baselines by 31.4%, 5.8%, 38.8%, 18.0%, 30.2%, 25.11% respectively on the six datasets. BatDiff also achieved  $\leq 18\%$  mean absolute percentage error (MAPE) on all datasets, meaning that BatDiff predicts relatively small errors for all cells under diverse prediction scenarios. In contrast, the baseline methods occasionally produce  $> 30\%$  MAPE, rendering them unsuitable for general applications.

Figure 3a demonstrates the comparison of deep models under different random seeds on the six datasets. Among the baselines, the multi-layer perceptron (MLP) demonstrates modest prediction errors with the lowest variance on average. The RMSE of the convolutional network (CNN) shows the largest variance, yet achieves the lowest errors in four

datasets among the baselines. Note that CNN becomes the strongest baseline when using the optimal seeds [2]. The long short term memory (LSTM) network achieves the best accuracy-variance trade-off. BatDiff outperforms these baselines in both accuracy and robustness. Figure 3b displays the instance-level prediction errors of BatDiff on MIX-100 dataset, where the absolute percentage error is lower than 20% for 84.7% cells. Figure 3c plots the cumulative absolute error with respect to the fraction of test samples in MIX-100 dataset. The error curves of the random forest (RF) and BatDiff initially coincide for the first approximately 50% of test samples, after which the error of RF begins to escalate at a faster rate than that of BatDiff. This suggests that RF accurately captures the patterns within a subset of the samples, whereas BatDiff excels at capturing the patterns in the remaining portion. Finally, the consistent slope of the error

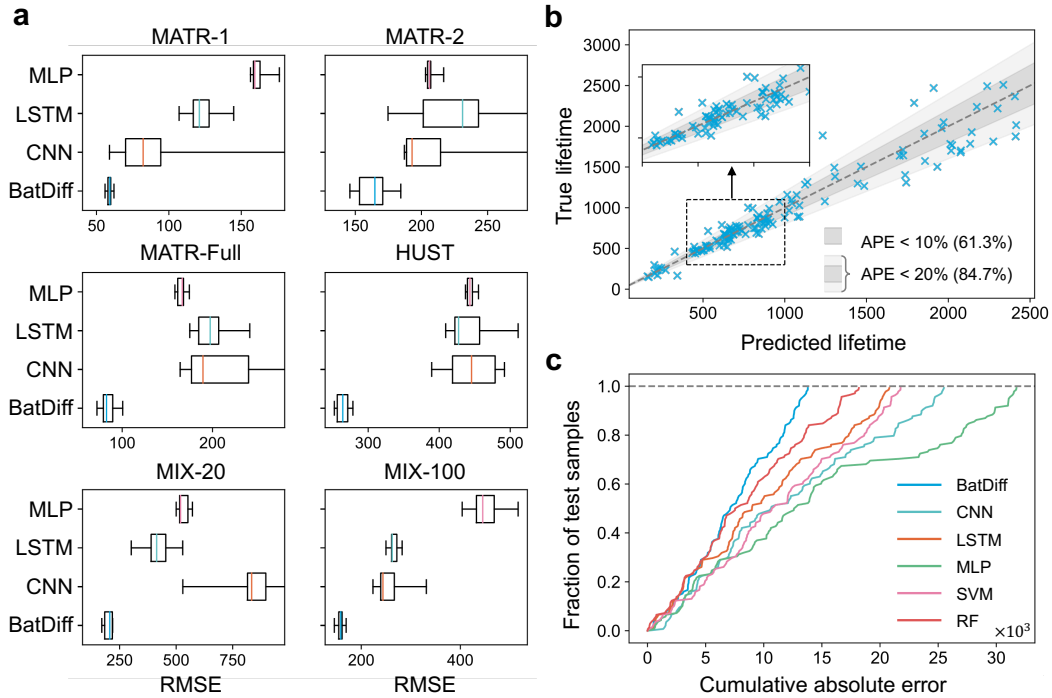


**Figure 3.** Visualization of comparison results. **a:** Performance of NN-based methods using different random seeds. CNN model exhibits larger variance than LSTM but sometimes achieves smaller errors. BatDiff is more accurate and robust to all baseline models. **b:** Prediction error for individual battery cells of MIX-100 dataset. **c:** Cumulative absolute error plotted with respect to the fraction of test samples used from MIX-100 dataset. Stronger models are those closer to the upper-left corner.

growth curve for BatDiff signifies that BatDiff does not exhibit excessively large prediction errors for any batteries.

#### 4 Mechanism of BatDiff

Here we conduct further ablation experiments to study the mechanism of BatDiff.

Figure 4a compares the predictive performance of different BatDiff branches. Across all datasets, IntraCD exhibit the highest error and variance. The InterCD-based model shows good robustness with lower variance across all datasets, yet its prediction accuracy is slightly lower than that of the IntraCD on some datasets, as its predictions are implicitly derived through the reference cells. The ensemble of the two separately trained branches obtains better performance on HUST and MIX-100, yet on other datasets it inherits the flaws of either branch, resulting in higher variance or suboptimal accuracy. BatDiff achieved the most robust and precise lifetime estimation across all datasets, demonstrating that through the co-training with shared prediction layers, the model better integrates the strength of both branches and yields the strongest predictive performance. Figure S7 shows their convergence curves, confirming that IntraCD-based model can easily overfit while InterCD converges robustly.

Figure 4b displays the performance of BatDiff when using a subset of the six capacity-indexed features. It’s evident that all six features play a crucial role in achieving improved predictive performance. The current-based features can lead to high variance and large errors, yet they are indispensable for the extreme early prediction scenarios in MIX-20. The voltage- and discharge-based features demonstrate strong performance across all datasets. Merging voltage and current features from both charge and discharge stages results in enhanced performance, with the best outcomes achieved by employing all six features.

We further investigated the mechanism of InterCD in a realistic battery testing scenario where we need to use the historical battery data to boost the prediction of a new battery type. We divided batteries in MIX-100 into four categories according to the electrode material, resulting in 225 LFP cells, 32 lithium cobalt oxides (LCO) cells, 61 lithium nickel manganese cobalt oxides (NMC) cells, and 19 lithium nickel cobalt aluminium oxides (NCA) cells. We assumed that the full life cycle data of the LFP batteries were known and employed them to assist the prediction of the other three types of batteries. Among these target types, we randomly sample a small fraction of batteries as training cells. The fraction is kept within 20% to mimic the limited testing cost in practice. We considered two learning enhancement methods. The first

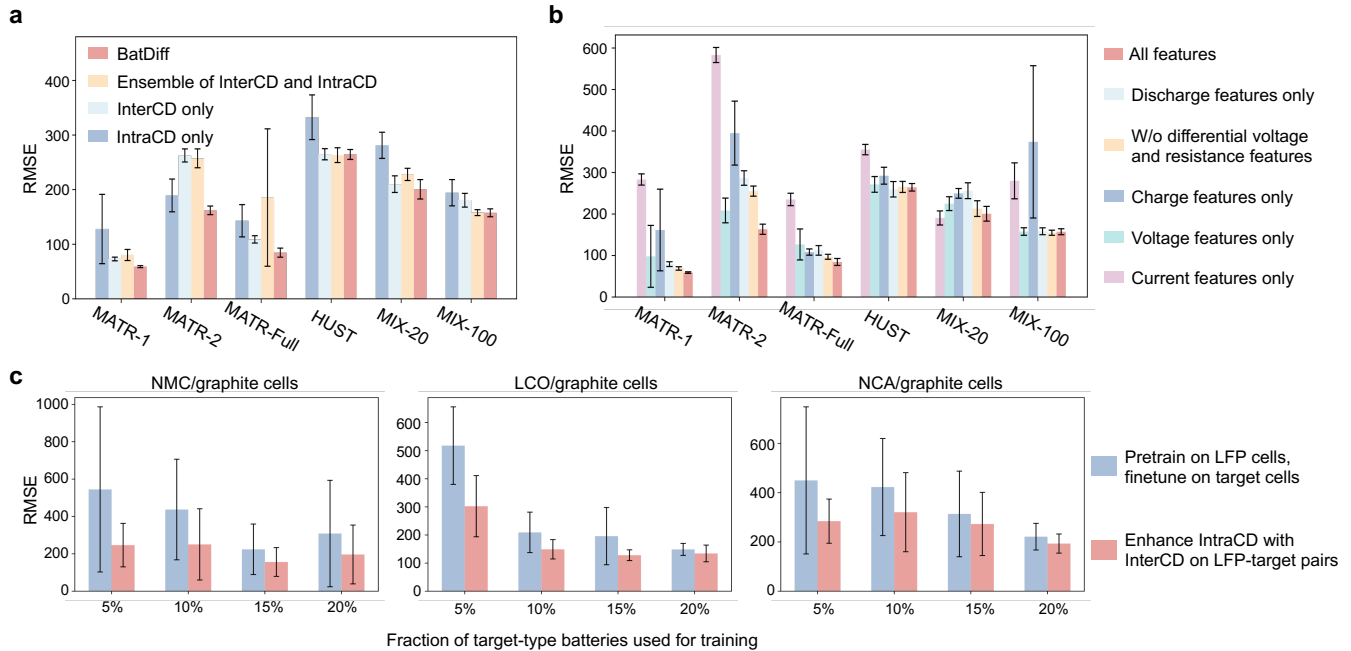


**Figure 4.** Ablation studies. **a:** Enhanced predictive performance necessitates the inclusion of the complete voltage and current signals, as well as their interactions, from both charging and discharging stages. **b:** Leveraging the joint training of IntraCD and InterCD branches, BatDiff achieves superior performance than the ensemble of IntraCD and InterCD models. **c:** Comparison of transfer- and InterCD-based methods that utilize historical data to enhance the prediction of new battery types. Employing the InterCD-based method to explicitly model battery interrelations leads to a substantial improvement in prediction performance for new battery types.

method was pre-training on LFP data and then fine-tuning on the target batteries, a typical transfer learning paradigm. The second method was to learn an InterCD model directly on the LFP-target battery pairs, and then ensemble with the IntraCD model trained on the limited target cells.

Figure 4c shows the comparison results on these three types of batteries. Compared to transfer learning, the InterCD-based model demonstrates a lower average error and significantly smaller variances on all three types of batteries. Notably, the performance gap between the transfer-learning and InterCD-based methods increases as we use less target cells. InterCD-based model even decreased the error by half compared to transfer learning when using only 5% of the data for training. This indicates that InterCD can make more effective use of existing data and thus is less sensitive to data scarcity issues. In practice, InterCD-based methods such as BatDiff can significantly reduce testing costs while ensuring prediction accuracy. This feature will greatly benefit downstream tasks, such as optimizing battery charging and discharging strategies or electrode materials.

## 5 Discussion

In this article, we present a novel framework named BatDiff for early battery lifespan prediction across diverse aging

conditions. While existing methods primarily rely on the intra-cell difference and struggle to generalize beyond target battery type and operating conditions, we proposed to utilize inter-cell difference features, regardless of the reference battery type, for superior battery life prediction. Our key insights are that the variations in electrical signals between the corresponding cycles of different batteries are strongly correlated with their lifetime difference, and the intra- and inter-cell difference can be seamlessly integrated to achieve accurate and robust predictions. We have curated all publicly available datasets, to the best of our knowledge, that are applicable to early lifetime prediction. These datasets are organized into six collections, which comprehensively cover a wide range of material types and operating conditions. BatDiff outperforms the best baselines by 31.4%, 5.8%, 38.8%, 18.0%, 30.2%, 25.11% respectively on the six test datasets rendering it an accurate and robust cross-condition battery lifetime predictor.

BatDiff showcases the considerable advantages of incorporating past battery data for battery degradation modeling. This innovative approach has the potential to significantly impact various applications beyond lifetime prediction in the battery industry, including but not limited to state of health and capacity estimation. By effectively reusing data from

previous research, BatDiff highlights the value of historical data scattered across different studies, emphasizing the importance of data sharing in the battery research community.

## 6 Methods

### 6.1 Capacity-indexed input feature space

For both IntraCD and InterCD, the construction of the feature space forms the foundation for accurate battery lifetime prediction. Electrochemical signals serve as the most suitable input for this task due to availability and non-invasiveness. To include the complete degradation information, the raw input feature space of BatDiff is exclusively based on the current and voltage signals during both charge and discharge periods.

For any battery, we first differentiate the charge and discharge periods by the sign of the current and integrates the current over time to obtain the capacity curves for both periods. We then interpolate the voltage and current signals from charge and discharge periods with respect to the capacity curve to obtain  $V(Q_d)$ ,  $V(Q_c)$ ,  $I(Q_d)$ ,  $I(Q_c)$ . To encapsulate information from both charge-discharge and voltage-current data, we additionally generate two features, namely the differential voltage-capacity curve  $V(Q_c) - V(Q_d)$  and the resistance-capacity curve  $R(Q) = \frac{V(Q_c) - V(Q_d)}{I(Q_c) - I(Q_d)}$ . As different battery types usually work with different nominal capacities, to properly calculate the InterCD features between different battery types, we normalize the capacity of all batteries using corresponding nominal capacities. This process ensures that the domain of the input features for all battery capacities is  $[0, 1]$ .

Depending on the specific charge-discharge strategy, these capacity-aligned curves can exhibit abrupt changes in current and voltage signals. Both IntraCD and InterCD computations can potentially produce spikes at these jump locations due to data misalignment. To eliminate the data noise introduced by these spikes, we employ a rolling-median-based filter for feature post-processing:

$$\mathbf{M} = \text{rolling\_median}(\mathbf{r}, w), \quad (1)$$

$$\Delta \mathbf{M} = \text{abs}(\text{rolling\_median}(\mathbf{M}, w)), \quad (2)$$

$$r_t^{new} = \begin{cases} M_t & \text{if } \Delta M_t > 3 \times \text{median}(\Delta \mathbf{M}), \\ r_t & \text{otherwise.} \end{cases} \quad (3)$$

Here  $\mathbf{r}$  is the raw signal and  $w$  represents the window size of the rolling operations.

### 6.2 Joint training of intra- and inter-cell difference

Figure 1b shows that the InterCD features are highly related to the battery life difference, which resides in the same linear space as the output of the IntraCD-based methods. This shared output domain allows performance enhancement through contrastive learning of the two branches.

We first consider two ideal linear models for IntraCD and InterCD with parameters denoted as  $\mathbf{w}$  and  $\boldsymbol{\theta}$ . Suppose the data are sampled from a distribution  $D$  that comprises batteries of the same type but random operating conditions. We assume that the first cycle  $\mathbf{x}_0$  for all batteries adopts the same charge and discharge protocols. Using this  $\mathbf{x}_0$  as the reference signal for IntraCD, we have

$$\mathbb{E}_{(\mathbf{x}, y) \sim D} \left[ y - \sum_{n=1}^N \mathbf{w}_n^T (\mathbf{x}_n - \mathbf{x}_0) \right] = 0, \quad (4)$$

$$\mathbb{E}_{(\mathbf{x}, y) \sim D, (\mathbf{x}', y') \sim D} \left[ (y - y') - \sum_{n=1}^N \boldsymbol{\theta}_n^T (\mathbf{x}_n - \mathbf{x}'_n) \right] = 0. \quad (5)$$

Simultaneously applying Eq. (4) on  $(\mathbf{x}, y)$  and  $(\mathbf{x}', y')$  gives

$$\begin{aligned} & \mathbb{E} \left[ y - \sum_{n=1}^N \mathbf{w}_n^T (\mathbf{x}_n - \mathbf{x}_0) - \left( y' - \sum_{n=1}^N \mathbf{w}_n^T (\mathbf{x}'_n - \mathbf{x}'_0) \right) \right] \\ &= \mathbb{E} \left\{ (y - y') - \sum_{n=1}^N \mathbf{w}_n^T [(\mathbf{x}_n - \mathbf{x}'_n) - (\mathbf{x}_0 - \mathbf{x}'_0)] \right\} \\ &= \mathbb{E} \left[ (y - y') - \sum_{n=1}^N \mathbf{w}_n^T (\mathbf{x}_n - \mathbf{x}'_n) \right] = 0. \end{aligned} \quad (6)$$

Here we used the fact that the batteries of the same type have equivalent initial states in expectation. By subtracting Eq. (6) from Eq. (5) we obtain

$$\mathbb{E}_{(\mathbf{x}, y) \sim D, (\mathbf{x}', y') \sim D} \left[ \sum_{n=1}^N (\mathbf{w}_n^T - \boldsymbol{\theta}_n^T) (\mathbf{x}_n - \mathbf{x}'_n) \right] = 0, \quad (7)$$

which indicates  $\mathbf{w}_n = \boldsymbol{\theta}_n$  for any cycle  $n$ .

Inspired by this equivalence, instead of introducing a contrastive loss that implicitly encourages the alignment of the output spaces, we decided to explicitly share the weights of the projection layer of the IntraCD and InterCD when adopting non-linear models to deal with batteries of varying types. To further ease the alignment of the embedding space of the two approaches, we employ the same architecture for their encoders to ensure a comparable fitting capability.

### 6.3 Choice of reference cell for InterCD

While the reference signals of IntraCD-based methods are restricted to its own cycles, InterCD-based methods allow flexible selection of reference batteries. This additional freedom enables us to enhance the predictive performance through the careful choice of reference cells.

Figure S5 demonstrates the substantial impact of different reference cell selection strategy on the prediction error for each battery for InterCD. The gap between the least favorable and optimal reference choices can lead to an absolute error exceeding 1500 cycles. The rules for the optimal reference choice of reference varies among the target batteries, as shown in Figure S6. In BatDiff, we employ the median of the predictions of a reference battery group of size 32

as the final prediction, which runs at 353 target batteries per second during inference. Using this reference ensemble strategy, both the mean and variance of the inference error decrease as the number of reference batteries increases. Impressively, this choice leads to a significant improvement compared to the worst-case scenario, resulting in an absolute error reduction of more than 1000 cycles for specific cells. However, a substantial gap still exists between the median choice and the optimal one. Closing this gap requires the model to intelligently select the most suitable reference cell for each battery. We provide more analysis about reference cells in the Supplementary Materials, and the search for the optimal reference choice is deferred to future work.

#### 6.4 Architecture design and experimental setups

The input features  $\mathbf{x}$  have dimensions of  $(B, 6, H, W)$ , where  $B$  represents batch size,  $H$  stands for cycle count, and  $W$  denotes the dimension of interpolated normalized capacity. The encoder contains two 2D convolutional layers, each followed by an average pooling layer and a ReLU activation layer. Different from computer vision applications, our use of average pooling allows the model to focus on the overall characteristics of the difference curves, rather than abrupt changes in specific locations such as spikes caused by data misalignment. The end of the encoder is a fully connected layer that compresses the spatial dimensions  $(H, W)$  to 1, facilitating subsequent predictions through the shared linear regression layer.

The metrics used in this work include the root mean square error (RMSE), absolute percentage error (APE), and the mean absolute percentage error (MAPE)

$$\text{RMSE}(\mathbf{y}, \hat{\mathbf{y}}) = \sqrt{\frac{\sum_{n=1}^N (y_n - \hat{y}_n)^2}{N}}, \quad (8)$$

$$\text{APE}(y_n, \hat{y}_n) = \left| \frac{y_n - \hat{y}_n}{\hat{y}_n} \right|, \quad (9)$$

$$\text{MAPE}(\mathbf{y}, \hat{\mathbf{y}}) = \frac{1}{N} \sum_{n=1}^N \text{APE}(y_n, \hat{y}_n). \quad (10)$$

Here  $\hat{\mathbf{y}}$  represents the ground truth labels and  $\mathbf{y}$  stands for the predictions.

We employ a hidden layer dimension of 32 across all models. For all neural network models, we conduct eight runs using random seeds ranging from 0 to 7 to evaluate their performance under different initialization conditions. In each experiment, 32 reference cells are employed for inference and we take the median of these reference cells as the final prediction for the InterCD branch. All experiments are executed on a server with 8 GTX 3090 GPUs, and we leverage PyTorch’s timer to conduct repeated runtime assessment.

## References

- [1] Peter M. Attia, Aditya Grover, Norman Jin, Kristen A. Severson, Todor M. Markov, Yang-Hung Liao, Michael H. Chen, Bryan Cheong, Nicholas Perkins, Zi Yang, Patrick K. Herring, Muratahan Aykol, Stephen J. Harris, Richard D. Braatz, Stefano Ermon, and William C. Chueh. Closed-loop optimization of fast-charging protocols for batteries with machine learning. *Nature*, 578:397–402, 2020.
- [2] Peter M. Attia, Kristen A. Severson, and Jeremy D. Witmer. Statistical learning for accurate and interpretable battery lifetime prediction. *Journal of The Electrochemical Society*, 168(9):090547, 2021.
- [3] Arnaud Devie, George Baure, and Matthieu Dubarry. Intrinsic variability in the degradation of a batch of commercial 18650 lithium-ion cells. *Energies*, 11:1031, 2018.
- [4] Wei He, Nicholas Williard, Michael Osterman, and Michael Pecht. Prognostics of lithium-ion batteries based on dempster–shafer theory and the bayesian monte carlo method. volume 196(23), pages 10314–10321, 2011.
- [5] Daniel Juarez-Robles, Judith A. Jeevarajan, and Partha P. Mukherjee. Degradation-safety analytics in lithium-ion cells: Part i. aging under charge/discharge cycling. *Journal of The Electrochemical Society*, 167:160510, 2020.
- [6] Weihai Li, Neil Sengupta, Philipp André Dechent, David Howey, Anuradha Annaswamy, and Dirk Uwe Sauer. One-shot battery degradation trajectory prediction with deep learning. *Journal of power sources*, page 230024, 2021.
- [7] Guijun Ma, Songpei Xu, Benben Jiang, Cheng Cheng, Xin Yang, Yue Shen, Tao Yang, Yunhui Huang, Han Ding, and Ye Yuan. Real-time personalized health status prediction of lithium-ion batteries using deep transfer learning. *Energy & Environmental Science*, 2022.
- [8] Yuliya Preger, Heather M. Barkholtz, Armando Fresquez, Daniel L. Campbell, Benjamin W. Juba, Jessica K. Román-Kustas, Summer R. Ferreira, and Babu R. Chalamala. Degradation of commercial lithium-ion cells as a function of chemistry and cycling conditions. *Journal of The Electrochemical Society*, 167:120532, 2020.
- [9] Kristen A. Severson, Peter M. Attia, Norman Jin, Nicholas Perkins, Benben Jiang, Zi Yang, Michael H. Chen, Muratahan Aykol, Patrick K. Herring, Dimitrios Fraggedakis, Martin Z. Bazant, Stephen J. Harris, William C. Chueh, and Richard D. Braatz. Data-driven prediction of battery cycle life before capacity degradation. *Nature Energy*, 4:383–391, 2019.
- [10] Nick Williard, Wei He, Michael Osterman, , and Michael Pecht. Comparative analysis of features for determining state of health in lithium-ion batteries. volume 4, pages 1–7, 2013.
- [11] Yinjiao Xing, Eden Ma, Kwok Leung Tsui, and Michael Pecht. An ensemble model for predicting the remaining useful performance of lithium-ion batteries. volume 53(6), pages 811–820, 2013.